The shape of a pulsar radio beam: fan beams, not the nested cones

Jarosław Dyks, Bronisław Rudak, Lab Saha, Marco Pierbattista
Nicolaus Copernicus Astronomical Center, Rabianska 8, Toruń, Poland

January 15, 2016

Abstract

We review the recently mounting evidence for the fan-shaped geometry of pulsar radio beams and we point at weaknesses of the nested cone model.

1 Fan beams explain components' bifurcations in radio pulse profiles

A simple argument for the fan beam geometry of pulsar radio emitter comes from observations of bifurcated emission components (BECs) in average radio profiles. Classical examples involve the trailing-side bifurcated component in the millisecond PSR J0437−4715 (Navarro et al. 1997; Oslowski et al. 2014; Dai et al. 2015) and the astonishingly symmetric double precursor of PSR J1012+5307 (Dyks et al. 2010, hereafter DRD10). Such features are also present in normal (non-millisecond) pulsars, eg. in the 5 GHz profile of B1933+16 (Mitra et al. 2016).

If we assume that geometry of emission region should be governed by the structure of the dipolar magnetic field, then BECs may be interpreted with two types of emitter: the conal one (a ring centered at the dipole axis, see top half of Fig. 1) and the fan beam limited to a narrow interval of magnetic azimuth (bottom half of Fig. 1). BECs (such as the one shown in the bottom right corner of Fig. 1) have dips (flux minima) at their centers, which implies a deficit of radiation in the central part of the emitter, as marked with the red stripes in Fig. 1. Note that to stay in the middle of an emitter, the dark stripes must extend at a fixed colatitude θ_m in the conal case (top), whereas they must occupy a fixed azimuth ϕ_m in the fan-beam case. We should observe the central dip in a BEC, when our line of sight is traversing through the dark (red) stripe. Only in the fan-beam case, however, the outstreaming plasma motion (directed away from the dipole axis) is expected to not smear the dip out. Since the lateral drift velocity is nonrelativistic ($v_d = c|\vec{E} \times \vec{B}|/B^2 \ll c$), the radio emitting plasma, when viewed down the dipole axis, streams mostly radially away from it (arrows in Fig. 1). In the conal case (top of Fig. 1), this motion is straight across the dark (red) stripe. For the dip in a BEC to survive, the plasma would have to stop emitting for a short while, when it is passing through the red stripe of diminished emission.

In the fan-beam case (Fig. 1, bottom), such a problem does not show up, because plasma moving within the red stripe may be consistently emitting less efficiently. Actually, when the fan-beam-emitting stream of charges is narrow in the magnetic azimuth, the bifurcation may still be present even when the emissivity is uniform in ϕ_m (ie. when the red stripe is missing). The bifurcation may then arise just from the bifurcated nature of the emitted microbeam. All the charges, whether within the dark stripe or outside, may have identical emissivity, albeit in the form of the bifurcated emission pattern (DRD10; also see fig. 1 in Dyks & Rudak 2012, hereafter DR12).

Thus, in the conal case the geometric arrangement of the emitter and plasma motion is expected to smear out any bifurcation, regardless of whether the microbeam is bifurcated or not. In the fan-beam case (narrow stream case) the bifurcation may survive regardless of whether the center of the stream is emitting less efficiently or not. If the red stream center is emitting as efficiently as its azimuthal peripheries, the bifurcation can still be produced by the form of the microbeam itself.

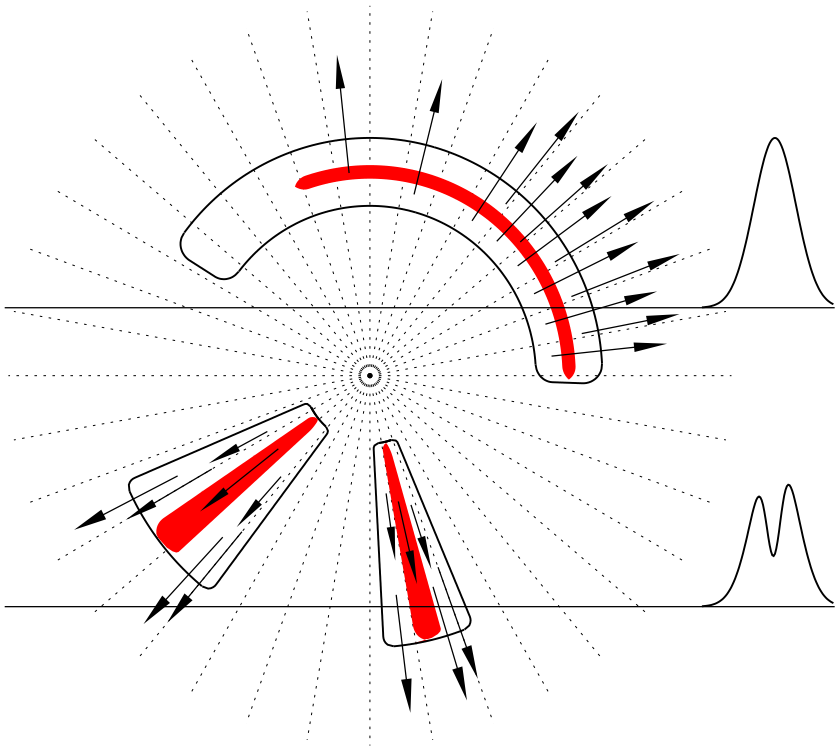

Figure 1: A head-on view (down the dipole axis) of radio pulsar beams in the fan beam model (bottom), and the conal model (top). The red stripes present the region of reduced emissivity, needed to explain the central minima in BECs. Horizontal lines mark the passage of sightline through the beams. Plasma outstreaming in the direction marked with arrows, is expected to smear out the bifurcation in the case of the conal model.

A third possibility (not shown in Fig. 1) is that the BECs may be produced by a fortunate cut of our sightline through tiny "minicones", ie. local conal subbeams with opening angles smaller than that of the overall polar tube (with a separate minicone for each BEC). Such conal subbeams could possibly be associated with local multipolar distortions of magnetic field. However, the BECs seem to be physically associated with double notches (DNs), which in J0437−4715 appear in the trailing wing of a BEC. The large observed depth of DNs can only be explained through a (missing) fan-shaped beam, not the conal one (see DRD10). Thus, by introducing the local conal subbeams, one would invoke two different geometries for a possibly related phenomena (BECs and DNs). The Ockham razor then suggests that such an idea of local conal beams (each single cone for each bifurcated component) is unlikely.

Therefore, out of those three geometrical interpretations, the fan beam (stream-generated) geometry, shown in the bottom part of Fig. 1, seems to be the most natural one for explaining both BECs and DNs. For this reason, it has been suggested that majority of radio pulsar profiles may need to be interpreted in terms of fan-beam shaped emitter (see sect. 6.4 in DRD10). Stream-shaped emitters (and fan beams) also appeared to be the right choice for Michel (1987), who argued for them based on circular polarisation data. Recent beam mapping for the precessing pulsar J1906+0746 (Desvignes et al. 2013) confirms all these geometrical arguments for the fan beam radio emission geometry.

2 Fan beams can do RFM

When the streams (and associated fan beams) are very narrow in magnetic azimuth, their emission is only detectable when our sightline is crossing the azimuth of the stream. In such a case, profiles should not exhibit the radius to frequency mapping (RFM), ie. the components should stay at a fixed phase at all frequencies ν (DR12). However, when the sky-projected pattern of intensity at a given ν is extended in ϕ_m and θ_m, the fan beams can produce RFM. A specific case of this is shown in Fig. 2 (from Dyks & Rudak 2015, hereafter DR15), which presents circular fixed-intensity patterns at different ν for four streams. In each stream, there is only one fixed-intensity contour shown for each frequency. The maximum intensity is at the center of each circle, and it drops down away from it (outward). The emission at any ν is not limited to the circle's interior, but extends further out,

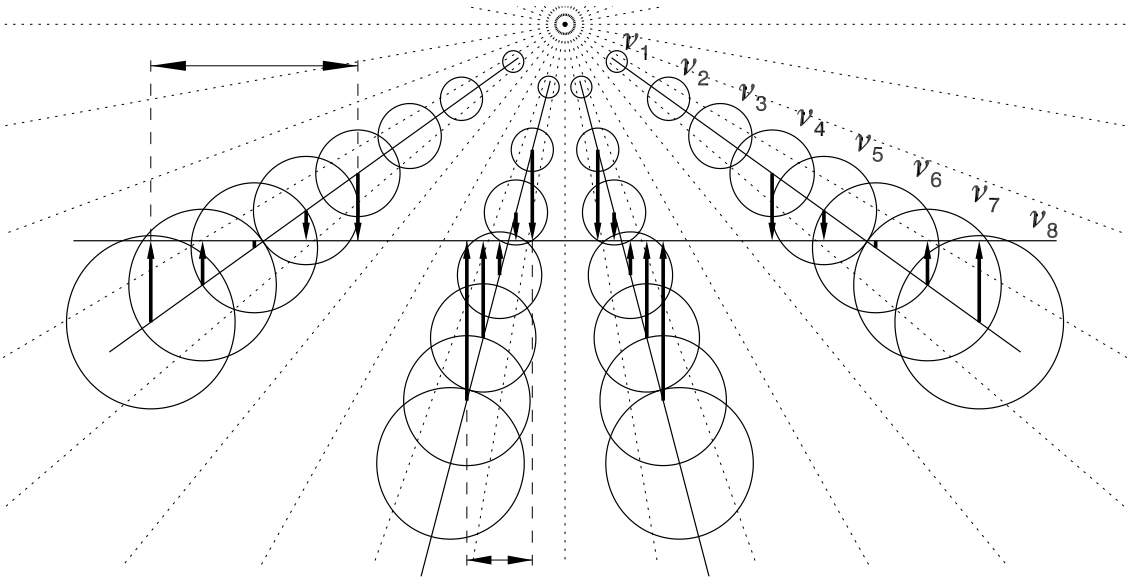

Figure 2: The mechanism of the apparent radius-to-frequency mapping. Circles of different size represent fixed-intensity contours at different frequencies, with the maximum intensity at the their centres. Pulse longitudes for components' peaks observed at different ν are marked with vertical arrows. The equidistant locations of the consecutive ν-contours (same for all beams) represent the same angular spectral gradient along all four beams. Note the smaller apparent RFM for the inner components (bottom horizontal arrow) as compared to the outer components (top horizontal arrow).

albeit at a decreasing level. Low-ν patterns peak further from the dipole axis, ie. at a larger θ_m. The observer, sampling the beam along the horizontal line, will see the components' peaks at the closest approach to a circle for a given ν. Hence, the observer will see a clear RFM, as marked with vertical arrows in Fig. 2. Moreover, since the inner streams are cut at a larger angle (nearly orthogonally), the same 'angular spectral gradient' along the streams will produce weaker RFM for the inner pair of components. This weaker spread of inner components is a well known phenomenon, previously interpreted through a less-flaring inner magnetic funnel of the nested cone model. Note that in the fan-beam model, all the streams may be identical, and anchored at the same distance from the dipole axis, but the effect will show up anyway. In the fan-beam model, the inner cone and the core beam (co-axial with the dipole axis) do not need to exist. According to the fan-beam model, the apparent RFM becomes weaker when the fixed ν patterns are more elongated in θ_m (see Fig. 3 in DR15), which explains why the millisecond pulsars, with their strongly flaring B-field lines, exhibit little RFM.

A similar RFM mechanism has been discussed within the fan beam model by Chen & Wang (2014) (cf. our Fig. 3 with their Fig. 13), as a possible explanation for the frequency evolution of profile outer widths.

3 Fan beams can produce the core-component lag.

Gupta & Gangadhara (2003) identified a group of pulsars in which the middle (or central) component (hereafter MC) lags the midpoint between pairs of outer, or flanking components (FCs). The MC lag is stronger for more peripheric pairs of FCs and it is also stronger for lower frequencies.

All these properties appear in the fan-beam model, because the aberration and retardation effects (AR), transform the system of fan beams into the swirl-like form shown in Fig. 3 (from DR15). This is because the AR are stronger at larger radial distance r, hence the forward swirl is stronger at larger angular distance from the dipole axis (θ_m). A clear advantage of the fan-beam interpretation of the MC lag, is that the lower emission altitudes (for the inner pair of FCs and for the MC) result naturally from the fact that inner streams are cut at a smaller θ_m (hence r), see Fig. 3. In the conal model, all the emission rings need to be 'manually' positioned at an appropriate r to explain the phenomenon.

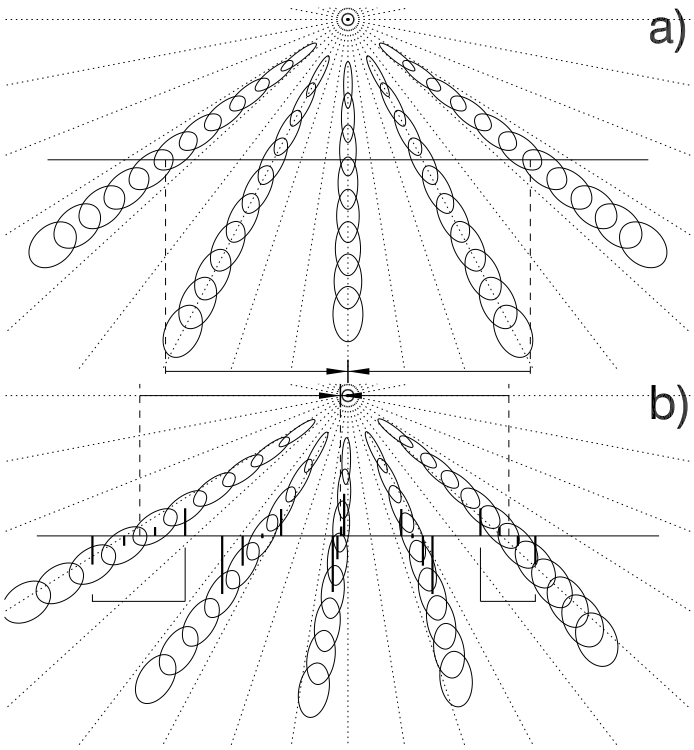

Figure 3: The mechanism of "core" lag with respect to centroids of outer components. **a)** A sky-projected emission beam with no aberration-retardation effects included. The ellipses present fixed-intensity contours at different frequencies, which decrease outwards. Emission altitude decreases towards the dipole axis. **b)** The beam with the AR-effects included. Note the forward bending of individual fan beams. All ellipses were shifted leftward by a θ_m-dependent interval $|\Delta\phi| \propto r \propto \theta_m^2$. The lag of the central component is marked with the horizontal arrows. Note that leading-side fan-beams are cut at a smaller angle than those on the trailing side. This implies the lag is larger at lower ν, through the mechanism shown in Fig. 2.

In the fan-beam model, the lag arises naturally. Again, there is no need for the "core" beam, coaxial with the dipole axis. The MC is just produced by the middle (probably most meridional) stream. The altitude differences for different components are likely much smaller than in the traditional conal model where the "core" is usually put near the neutron star surface. More details on how the fan-beam model works for the MC lag, along with the mathematical description, can be found in Section 5.2 of DR15.

4 Fan beams explain the statistics of profile morphology better than cones

Statistics of pulse profile widths, measured at a low flux level or between the peaks of outermost components, has been extensively studied within the conal model (Rankin 1993; Gil & Kijak 1993; Kramer et al. 1994; Mitra & Deshpande 1999). Most of these works merged at a common conclusion that pulsar beams consist at most of two nested cones of emission, with additional central core beam possible. The angular radii of the cones have been established to have a universal size ratio: $R_\rho = \rho_{in}/\rho_{out} \approx 0.75$, which actually can be supported on theoretical ground (Wright 2003). However, this result has been obtained with conal-model-based methods which are highly capable of adjusting to observations, even if some of parameters are assumed wrong. The observed width of a profile depends on the physical width of the emitter (depending on r and ν), dipole tilt, sightline impact angle and pulsar period, most of which are unknown and convolved with each other.

To overcome this problem, it is worth to work on the *ratio* of components' separations ($R_W = W_{in}/W_{out}$), instead of the separations (widths) themselves (see Dyks & Pierbattista 2015). Here W_{in} and W_{out} denote the observed peak-to-peak separations observed between the "conal" components in the inner and outer pair, respectively. Both values can be measured for a single object, if its profile is of Q, or M type, ie. if it contains at least four components. Taking R_W instead of W is useful, because both W_{in} and W_{out} depend in a nearly identical way on dipole tilt and others above-mentioned parameters, so this dependence calcels out in their ratio. This way the method becomes independent of most unknown factors, which are difficult or impossible to determine. The main disadvantage of

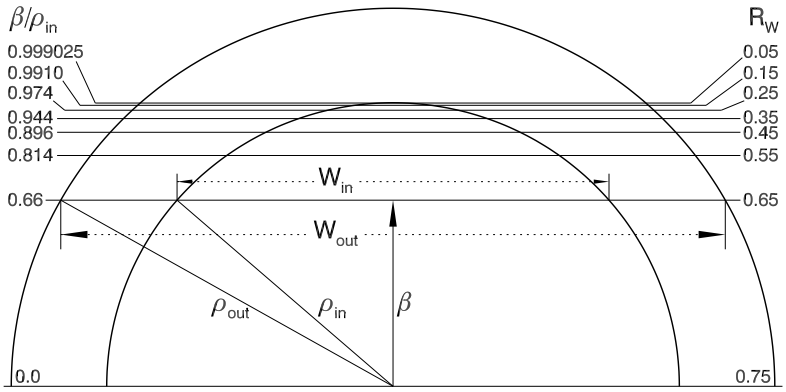

Figure 4: Top half of a nested cone beam (two half-circles) with the cone size ratio $R_\rho = 0.75$. The set of horizontal lines (paths of different sightlines) presents intervals of viewing angle that correspond to a fixed interval of the peak-separation ratio $\Delta R_W = 0.1$. Values of the impact angle β (in units of the inner conal radius ρ_{in}) are given on the left, values of R_W – on the right hand side. Note that it is a lot more probable to observe $R_W \in (0.65, 0.75)$ than the smaller values.

this method is the limited number of known Q and M pulsars, as well as problems with identification of blended components.

The afore-mentioned nested cone geometry predicts unique distribution of R_W values. This distribution is a result of different viewing impact angles β and does not much depend on any other geometrical parameters. As illustrated in Fig. 4, and 5a, the distribution is dominated by values of R_W which are close to the maximum $R_\rho \approx 0.75$. Smaller values of R_W only appear for peripheric traverse through the beam, which is much less likely. This conal distribution of R_W is in total disagreement with the observed one, shown in Fig. 5c (KS probability of consistency: 10^{-12}).

On the contrary, even the simplest fan-beam model predicts the R_W distribution which is much less dissimilar to the observed one (KS prob. of a few times 10^{-3}, see Fig. 5b). This fan-beam result has been obtained for a simple system of ten fan beams (five in the poleward, and five and the equatorward part of the polar region) of uniform emissivity and zero width (each fan beam is represented by a single value of randomly-selected magnetic azimuth). Both models can be made more similar to data by introducing parameters which govern observational selection effects, however, the natural tendency of fan-beams to produce the wider distribution of R_W, which is more consistent with the data, is obvious.

Other (independent) statistical arguments for the fan beam model have recently been presented in Wang, Pi, Zheng, et al. (2014). They have shown that the observed distribution of profile widths as a function of the impact angle is more consistent with the fan beam, rather than the conal geometry.

5 Conclusions

Fan beams have appeared to be very successful in interpreting the bifurcated features in radio pulse profiles. Actually they were shown to be indispensable for understanding the double notches (DRD10), and provide the most reasonable origin for the BECs. This is why some of us dared to propose that the traditional, conal classification scheme of pulsar profiles, would be better replaced with systems of fan beams (see Fig. 18 in DRD10). Since that time, evidence for fan beams has only been steadily increasing. It is now known that in accordance with observations, fan beams can produce RFM of magnitude which increases towards the profile periphery. Fan beams can also produce the MC lag with several observed properties, and they do so in a more natural way than the nested cone beam. Increasing number of statistical tests (R_W distribution, pulse width versus impact angle distribution) confirm the fan beam geometry. First beam maps of precessing objects (Desvignes et al. 2013; Manchester et al. 2010) are also consistent with the azimuthally limited beams. More support for the fan beam system is on the way.

With no hesitation we repeat our claim that systems of fan beams offer a better model for pulsar radio beams, than the nested cone geometry. It is a high time to change the traditional paradigm of pulsar radio emission geometry.

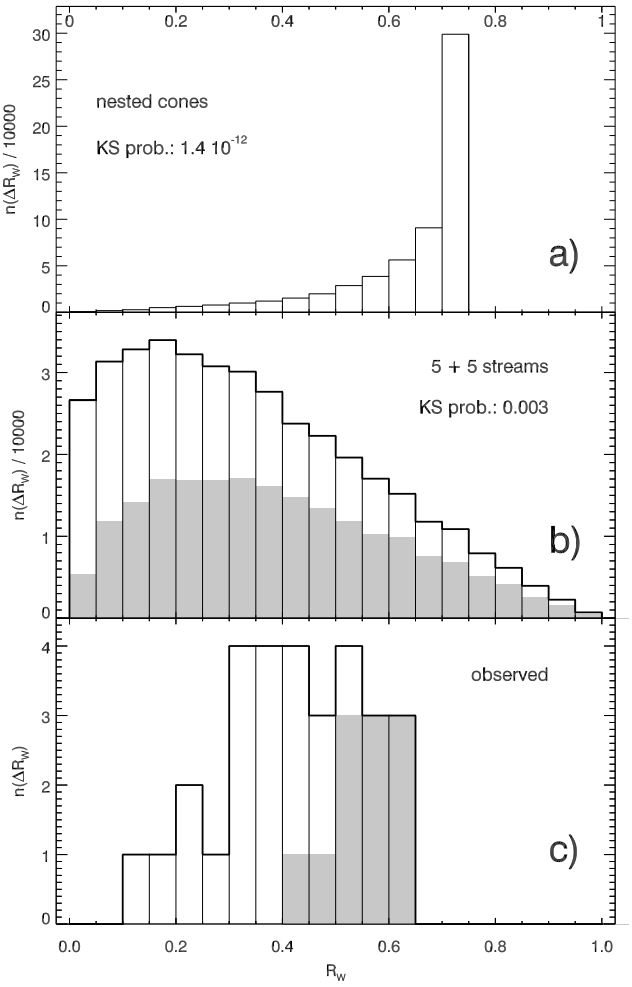

Figure 5: Comparison of the simulated R_W distributions (conal model in panel a; fan beam model in b) with the one observed for Q and M type pulsars (panel c). The numbers in a and b give the KS probablity of consistency with the observed distribution. Note the low likelihood of the conal model. Grey parts of the histograms in b and c denote the M-type profiles. An unknown fraction of these is also included in the histogram of panel a, which shows the sum of the Q and M profiles.

6 Acknowledgments

This work has been funded by the National Science Center (Poland) as a project numbered DEC-2011/02/A/ST9/00256.

References

[1] Chen J. L., Wang H. G., 2014, ApJS, 215, 11

[2] Dai S., Hobbs G., Manchester R. N., et al., 2015, MNRAS, 449, 3223

[3] Desvignes G., Cognard I., Champion D, et al. 2013, in van Leeuwen J., ed., IAU Symp. Vol. 291

[4] Dyks J., & Pierbattista M., 2015, MNRAS, 454, 2216

[5] Dyks J., & Rudak B., 2012, MNRAS, 420, 3403 (DR12)

[6] Dyks J., & Rudak B., 2015, MNRAS, 446, 2505 (DR15)

[7] Dyks J., Rudak B., & Demorest P., 2010, MNRAS, 401, 1781 (DRD10)

[8] Gil J., & Kijak J., 1993, A&A, 273, 563

[9] Gupta Y., & Gangadhara R.T. 2003, ApJ, 584, 418

[10] Kramer M., Wielebinski R., Jessner A., et al., 1994, A&AS, 107, 515

[11] Manchester R. N., Kramer M., Stairs I. H., et al. 2010, ApJ, 710, 1694

[12] Michel F. C., 1987, ApJ, 322, 822

[13] Mitra D., & Deshpande A. A., 1999, A&A, 346, 906

[14] Mitra D., Rankin J., Arjunwadkar M., 2016, MNRAS, submitted

[15] Navarro J., Manchester R. N., Sandhu J. S., Kulkarni S.R., Bailes M., 1997, ApJ, 486, 1019

[16] Oslowski S., van Straten W., Bailes M., et al., 2014 MNRAS, 441, 3148

[17] Rankin J.M., 1993, ApJ, 405, 285

[18] Wang H. G., Pi F. P., Zheng X.P., et al., 2014, ApJ, 789, 73

[19] Wright, G. A. E., 2003, MNRAS, 344, 1041